3D Finite Element Modeling of Electromagnetic Forming Processes[*]

Ph. Conraux[1], M. Pignol[2], V. Robin[2], J.M. Bergheau[3]

[1] ESI Group, Lyon, France
[2] ESI France, Lyon, France
[3] LTDS, UMR 5513, CNRS/ECL/ENISE, St Etienne, France

Abstract

In the electromagnetic forming process (EMF, also known as magnetic pulse forming) the metal is deformed by applying a pressure generated by an intense, transient magnetic field. A great deal of research and investigation efforts are needed for gaining better understanding on the deformation mechanism in order to develop a suitable forming strategy and equipment. One way to reach this target is to employ suitable FE software to model the process. This investigation was partly conducted in the framework of a European project called EMF (G3RD-CT-2002-00798).

The first part of the paper presents the relevant physical phenomena which govern the EMF process and their interactions. The physical coupling principle as well as the required numerical models are also established. In the second section some cases for which the so developed code can be used for virtual testing is presented for validation. Finally, numerical results are compared with experiments on a 3D model, highlighting the interest of numerical modeling for process improvements.

Keywords:

Finite element method (FEM), Electromagnetic forming, Process modeling

1   Introduction

Electromagnetic forming requires the generation of a high and transient magnetic field by using an appropriate electrical device bringing energy of about hundreds of kJ [1]. This

---

field is developed in the surrounding of the forming coil and the metallic object to be formed. Like any other forming process, a die might be necessary to give the workpiece the required final geometry. The high current pulse passing through the coil produces eddy currents in the opposite direction to the process current that causes repulsive forces between the two components due to Lorentz forces. Modeling such a forming process requires the coupling of multiphysical phenomena, as described in Figure 1.
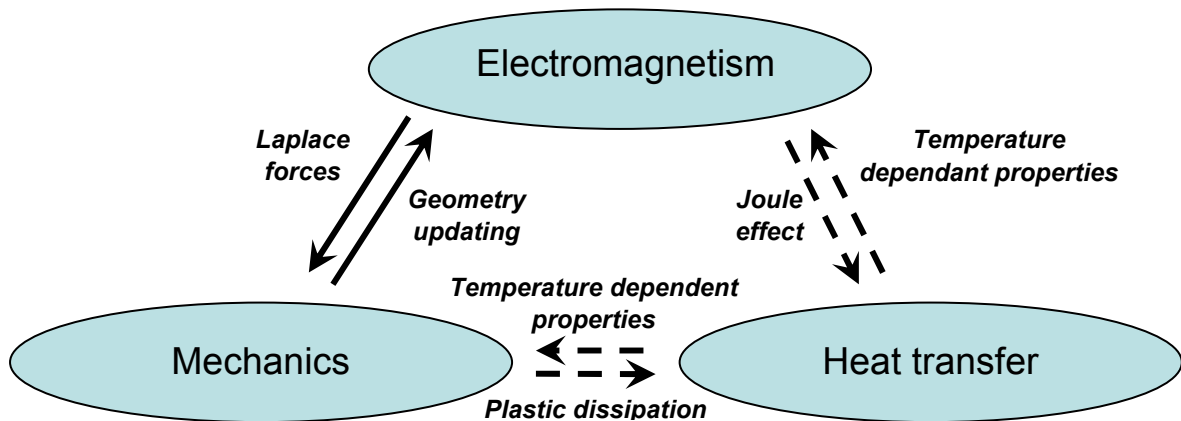
Figure 1: *Interaction between involved physical phenomena*

The effect of temperature variations was considered to be negligible for the simulation of the stamping process unlike some other approaches [2]. Indeed, temperature effects are very localized. Eddy currents generate a high thermal power density in a very short time so that heat transfer cannot affect the complete workpiece. The plastic work is distributed in the whole plastically deformed part of the component and does not need to be considered for more than classical stamping process.

ESI group's commercial finite element software solution is designed to model such a complex process. SYSMAGNA [3] can especially solve the electromagnetic part. PAMSTAMP code [4], dedicated to the stamping process simulation, is chosen for the structural analysis. In order to realize 3D simulations, some developments were performed in this software. The first part of the paper details the constitutive equations that govern electromagnetism and introduces the formulation of the 3D magnetodynamic problem.

The second part of the paper deals with some examples of application like tube compression test and plates, for which virtual testing is very efficient in order to optimize coil geometry or process parameters. A 3D non-rotationally symmetric component has been designed and its modeling finally demonstrates the now accomplished feasibility of 3D simulation of electromagnetic forming processes.

2   Electromagnetism finite element modeling

2.1   Maxwell equations

The electromagnetism phenomena are governed by Maxwell's equations. For sinusoidal currents whose frequency is in the order of 10^{12}Hz, displacement currents can be neglected and so the equations to be solved reduce to

$$curlH = J \tag{1}$$

$$curlE = -\frac{\partial B}{\partial t} \tag{2}$$

$$divB = 0 \tag{3}$$

where **H** is the magnetic field, **B** is the magnetic induction or magnetic flux density vector, **E** is the electric field, and **J** is the current density.
Constitutive material behavior laws relate these quantities together such as the magnetization law (4) and the Ohm's law (5).

$$B = \mu\left(\|H\|, \theta\right) \cdot \left(H\right) \tag{4}$$

where μ is the magnetic permeability that can depend considerably on temperature (Curie point) and on $\|H\|$.

$$J = \sigma(\theta)E \tag{5}$$

where σ is the electric conductivity which depends on temperature.
In order to solve this system of equations, the magnetic vector potential **A** is introduced from equation (3)

$$B = curlA \tag{6}$$

To ensure the uniqueness of **A**, a gauge condition (7) is mandatory (Coulomb's gauge):

$$divA = 0 \tag{7}$$

Equation (2) with relation (6) gives

$$E = -\frac{\partial A}{\partial t} - gradV \tag{8}$$

In equation (8), **E** is not uniquely defined because it depends on the electric scalar potential **V** that leads to an introduction of the conservation of current density (9) from equation (1).

$$div(J) = 0 \tag{9}$$

2.2 Partial differential problem

Finally, the system of equations to be solved is the following:

$$\sigma\left(\frac{\partial A}{\partial t} + gradV\right) + curl(v\ curlA) = 0 \tag{10}$$

$$div\left(\sigma\left(\frac{\partial A}{\partial t} + gradV\right)\right) = 0 \tag{11}$$

$$divA = 0 \tag{12}$$

where $\upsilon = \dfrac{1}{\mu}$ is the magnetic reluctivity.

The different boundary conditions possible in a bounded domain Ω with boundary $\partial\Omega = \partial\Omega_A \cup \partial\Omega_H = \partial\Omega_V \cup \partial\Omega_j$ are:

- Pescribed magnetic vector potential that can depend on time

$$A(t) = A^d(t)\ on\ \partial\Omega_A \tag{13}$$

- Prescribed electric potential

$$V(t) = V^d(t)\ on\ \partial\Omega_V \tag{14}$$

- Prescribed tangential magnetic field (with *n* being the outward unit normal to the surface)

$$H(t) \times n = H^d(t)\ on\ \partial\Omega_H \tag{15}$$

- Prescribed surface current density

$$-J \cdot n = \sigma\left(\frac{\partial A}{\partial t} + gradV\right) \cdot n = j^d\ on\ \partial\Omega_j \tag{16}$$

2.3 Finite element formulation

The variational problem consists in finding *A* and *V* such as:

$$\forall \mathbf{A}^*,\ \mathbf{A}^* = 0\ on\ \partial\Omega_A\ and\ \forall V^*, V^* = 0\ on\ \partial\Omega_V$$

$$\int_\Omega A^* \cdot \sigma\left(\frac{\partial A}{\partial t} + gradV\right)dv + \int_\Omega curlA^* \cdot v.curlA\ dv + \alpha\int_\Omega divA^*.divA\ dv - \int_{\partial\Omega_H} A^*.H^d\ ds = 0 \tag{17}$$

$$\int_{\Omega} gradV^* . \sigma . \left(\frac{\partial A}{\partial t} + gradV \right) dv - \int_{\partial \Omega_j} V^* . j^d ds = 0 \tag{18}$$

This formulation leads to the following first order partial differential system of equations.

$$\begin{Bmatrix} \Psi_A(\mathbf{A}, V) \\ \Psi_V(\mathbf{A}, V) \end{Bmatrix} = \begin{Bmatrix} \mathbf{R}_A(\mathbf{A}, V) \\ \mathbf{R}_V(\mathbf{A}, V) \end{Bmatrix} - \begin{bmatrix} \mathbf{C}_{\mathbf{AA}} & 0 \\ \mathbf{C}_{V\mathbf{A}} & 0 \end{bmatrix} . \begin{Bmatrix} \dot{\mathbf{A}} \\ \dot{V} \end{Bmatrix} = \begin{Bmatrix} 0 \\ 0 \end{Bmatrix} \tag{19}$$

with

$$\{\mathbf{R_A}\} = \mathop{\mathbf{A}}_{elements} \{\mathbf{R_A^e}\} \quad \{\mathbf{R}_V\} = \mathop{\mathbf{A}}_{elements} \{\mathbf{R}_V^e\}$$

$$[\mathbf{C_{AA}}] = \mathop{\mathbf{A}}_{elements} [\mathbf{C_{AA}^e}] \quad [\mathbf{C}_{V\mathbf{A}}] = \mathop{\mathbf{A}}_{elements} [\mathbf{C}_{V\mathbf{A}}^e] \tag{20}$$

$$\begin{aligned} \{\mathbf{R_A^e}\} \quad = \quad & \int_{\partial\Omega^e \cap \partial\Omega_\mathbf{H}} [N^e]^T H^d \, ds \\ - \quad & \int_{\Omega^e} [curlN^e]^T . v \, curlA \, dv - \alpha \int_{\Omega^e} [divN^e]^T divA \, dv \\ - \quad & \int_{\Omega^e} [N^e]^T . \sigma . gradV \, dv \end{aligned}$$

$$\begin{aligned} \{\mathbf{R}_V^e\} \quad = \quad & \int_{\partial\Omega^e \cap \partial\Omega_j} [N^e]^T j^d \, ds \\ - \quad & \int_{\Omega^e} [gradN^e]^T . \sigma . gradV \, dv \end{aligned}$$

$$[\mathbf{C_{AA}^e}] = \int_{\Omega^e} [N^e]^T . \sigma [N^e] dv \quad [\mathbf{C}_{V\mathbf{A}}^e] = \int_{\Omega^e} [gradN^e]^T . \sigma [N^e] dv$$

In the equations above, $\begin{Bmatrix} \mathbf{A} \\ V \end{Bmatrix}$ gather all degrees of freedom (dof) of the problem. 4 dof (A_x, A_y, A_z, V) are related to each node of the mesh. $\mathop{\mathbf{A}}_{elements}$ is the assembling operator of the elements. $[N^e]$ represents the shape functions of the element, $[gradN^e]$, the shape function gradient, and $[curlN^e]$ the shape function curl in such a way that inside each element $A = [N^e]\{\mathbf{A}\}$, $V = [N^e]\{V\}$, $gradV = [gradN^e]\{V\}$, and $curlA = [curlN^e]\{A\}$.

Equations (19) are solved step by step in time using an implicit backward Euler method. At each time step the solution is obtained through a Newton-Raphson procedure.

3 Validation examples

3.1 Mechanical behavior law

The sheet and tube specimens used for validation are aluminum alloys AA5754, AA5182, and AA6016. Their flow behavior needs to take into account high strain rates and the so-called Johnson-Cook model (21) is then used [5]. The model can also consider the influence of temperature, but this term is neglected for the simulation.

$$\sigma = \left(A + B\left(\varepsilon_{eq}^{p}\right)^{n}\right)\left(1 + C \ln \dot{\varepsilon}_{eq}^{*}\right)\left(1 - T^{*m}\right)$$

(21)

with

$$\dot{\varepsilon}_{eq}^{*} = \frac{\dot{\varepsilon}_{eq}}{\dot{\varepsilon}_{0}} \quad \text{and} \quad T^{*} = \frac{\theta - T_{ref}}{T_{melt} - T_{ref}}$$

$\dot{\varepsilon}_{eq}^{*}$ is the strain rate without dimension with $\dot{\varepsilon}_{0}$ usually set to 1.0s^{-1}. T_{melt}, T_{ref}, and θ respectively represent the fusion temperature, a reference temperature as room temperature, and the media temperature.

The parameters of the Johnson-Cook material behavior law has been identified at the Department of Material Engineering of the University of Trento in Italy.

3.2 Virtual testing

The experiments have been conducted at the Department of Forming Technology at the University of Dortmund in Germany. The experimental results are compared to the ones obtained by calculation. The isotropic plastic behavior of the workpiece is governed by the Johnson-Cook law. The electromagnetic behavior is also isotropic. No material non-linearity is considered for the electromagnetism simulation.

3.2.1 Tube compression tests

The geometry and the mesh are presented in Figures 2a and 2b. The surrounding air is meshed in order to propagate the magnetic field generated by the coil. The tube is made of AA5754 aluminum alloy. The charging energy is about 500J. The current applied to the coils becomes null after 200µs and, thus, the coupling between electromagnetism calculation and mechanical analysis is carried out each 2µs.
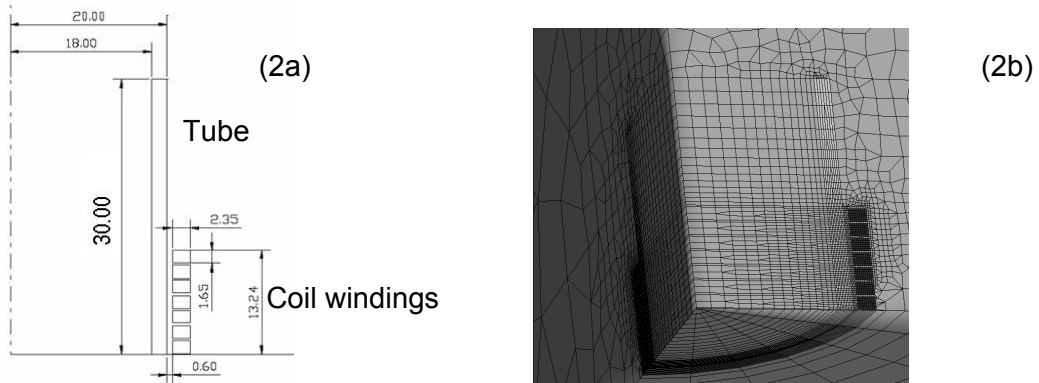
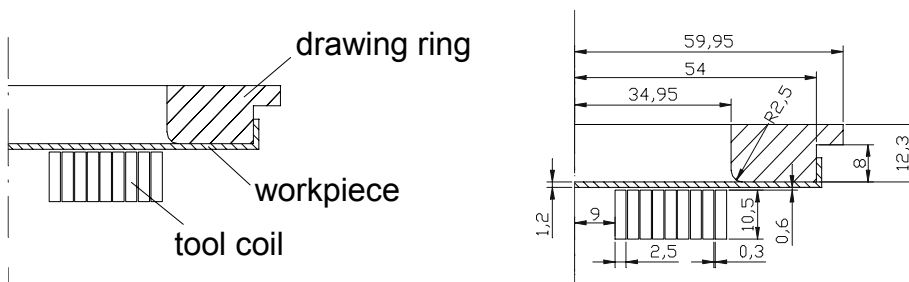Figure 2: Tube test geometry description (2a) and related 3D mesh (2b)

Figure 3 gives the maximal diameter reduction versus time. Experiments are compared to the numerical results and both are really in good agreement.
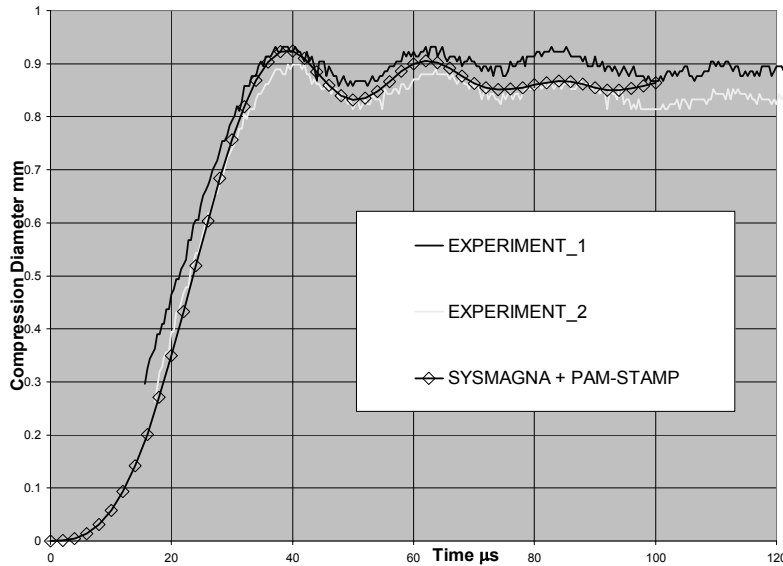

Figure 3: Diameter reduction as a function of time

3.2.2 Plate tests

The geometry of the plate test specimen is shown in Figure 4.

Figure 4: Geometry description of the plate test specimen

79

The sheet is made of AA5182 aluminum alloy. The charging energy is about 1200J. The coupling time step is 2μs. For this simulation contact conditions need to be considered between the plate and the drawing ring as it influences the way the workpiece is deforming.
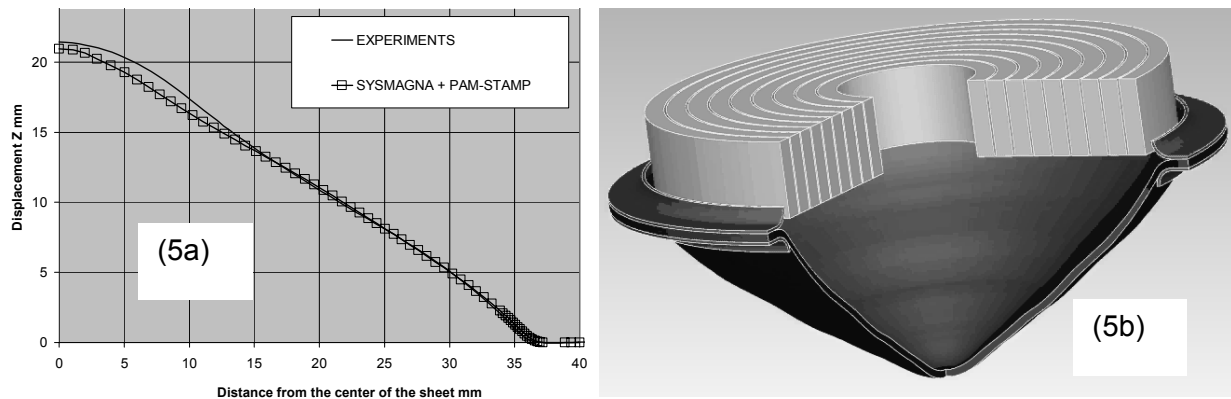

Figure 5: *Deformation at the end of the process*

Figures 5a and 5b give the displacements of the outer surface of the plate according to the distance from its centre and the deformed shape at the end of the process respectively. Experimental results and calculated displacements are very close to each other.

3.3   Industrial validation

This paragraph highlights all the technical functionalities of the software used to model the electromagnetic forming process. Indeed, the proposed validation of the industrial example is non-rotationally symmetric and a die is required to accurately obtain the final deformed shape. The die is oval, as shown in Figure 6, and the coil is designed according this shape.
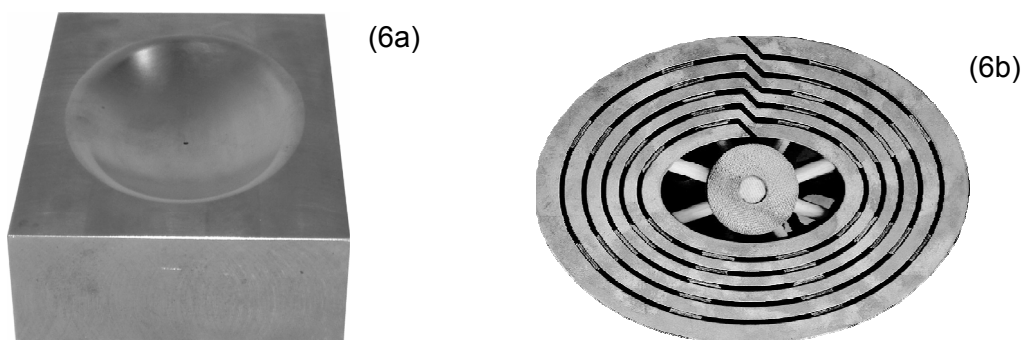

Figure 6: *Die (6a) and coil (6b) geometries*

The sheet is made of AA6016 aluminum alloy. Two charging energies were tested for this component. With a charging energy of about 2100J the required deformed shape is not obtained. So, the comparison between experiments and calculations focuses on the

process performed with the highest energy. Experimentally, the final geometry does not fit the die. Numerically, the results emphasize the same phenomena, as shown in Figure 7a along the major axis and 7b along the minor one.
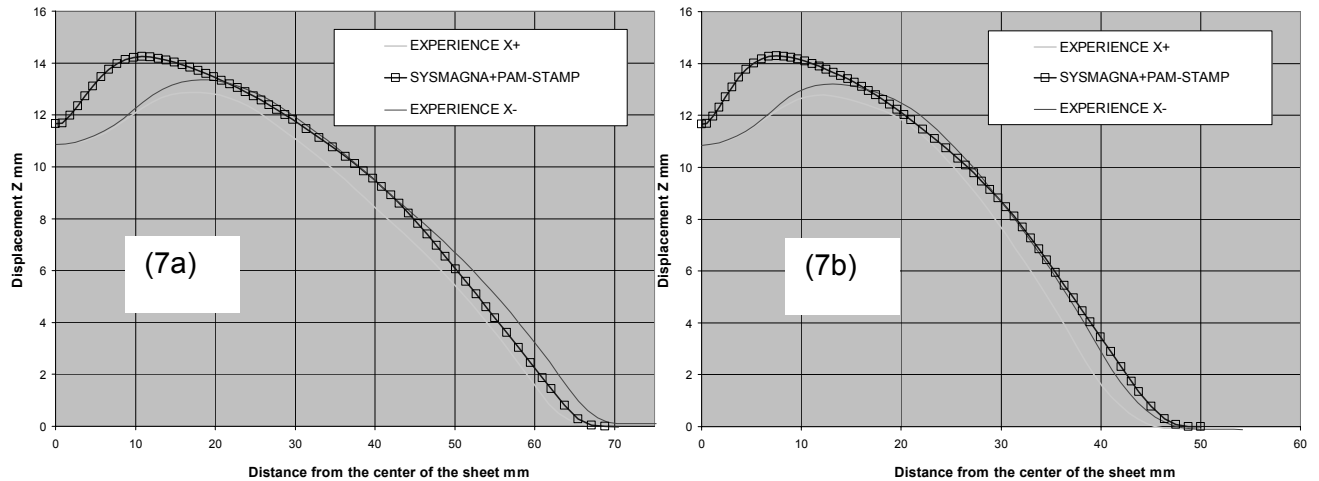
Figure 7: *Displacement at the end of the process along the major axis (7a) and the minor axis (7b)*

4   Conclusions

The efficiency of the fully 3D coupled numerical modeling of an electroforming process for virtual testing has been demonstrated. Indeed, experiments and computations correlate with each other, which validates the assumption made on temperature effects. Another approach should consist in combining the finite element method and boundary element method in order to get rid of the difficulty of meshing. Modeling movable parts involves to take care of the mesh density of the surrounding air. Sometimes, remeshing cannot be prevented. If the boundary element method makes the work easier in this case, it generally also leads to higher CPU costs directly related to the number of nodes on the boundary. For tube or sheet virtual testing CPU time is less than one hour using a personal computer (Pentium 4 and 2GHz) when the air is meshed. The required RAM is about 500Mbytes. Finally, concerning the tube compression test, the advantage of 3D analyses compared to 2D ones is the capability to predict the wrinkling effect due to a local reduction of the thickness of the tube or a non-perfect round tube. The highly dynamic nature of deformations involved during electroforming processes has the ability to improve the formability of aluminum more than conventional forming. Nevertheless, the alloy can exceed its forming limit and fracture. This other kind of defect can also be numerically predicted by including fracture mechanics to detect a crack initiation and the way it propagates [6].

References

[1]   *Psyk, V.; Beerwald, C.; Kleiner, M; Beerwald, M; Henselek, A*: Use of electromagnetic forming in process combination for the production of automotive part. Proceedings of the 2nd European Pulser Power Symposium, Hamburg, September 2005.

[2]   *Karch, C.; Roll, C.*: Transient simulation of electromagnetic forming of aluminium tubes. Proceedings of the 11th International Conference on Sheet Metal, Nürnberg, April 2005.

[3]   SYSWELD®, User's manual, ESI Group, 2005.

[4]   PAM-STAMP®, User's manual, ESI Group, 2005.

[5]   *Johnson, G.R.; Cook, W.H.:* A constitutive model and data for metals subjected to large strains, high strain rates and high temperature. Proceedings of the 7th International Symposium on Ballistic, 1983, p. 541.

[6]   *Kamoulakos, A.; Culiere, P.; Araki, T:* Prediction of ductile metal rupture with the E-W model in PAM-CRASH. Proceedings of the International Body Engineering Conference, Chiba, October 2003.